WIDEBAND VIBRATION ENERGY HARVESTING UTILIZING NONLINEAR SPRINGS

Duy Son Nguyen and Einar Halvorsen
Institute for Microsystem Technology, Vestfold University College, Norway

Abstract: Based on modeling and simulation, this paper investigates the use of nonlinear beams to extend the bandwidth of vibration energy harvesters. We have designed an electrostatic device with an asymmetric nonlinear suspension. A lumped model of the device, which we have implemented in a circuit simulator using parameters obtained from finite element analysis, is presented. We find that the harvester exhibits jumps during frequency and amplitude sweeps and broadening of the spectrum with increasing levels of broadband excitation. Our results show that considerable bandwidth enhancements can be achieved by utilizing nonlinear springs.

Keywords: energy harvester, nonlinear systems, electrostatic devices, vibrations.

INTRODUCTION

Designing energy harvesters to harvest energy from environmental motion with stochastic or varying vibration spectra has been a challenge. In our previous work [1], an in-plane overlap varying device with a nonlinear spring that displays both softening and stiffening behavior achieved a noticeable bandwidth enhancement without replying on impact of mechanical stoppers, resonance tuning or large electromechanical coupling. While impact on elastic stoppers [2] has much the same effect as stiffening springs, softening springs are different. In particular softening spring effects are interesting because they potentially allow larger displacements and suppress the dominance of mechanical over electrostatic forces.

Motivated by the experiments, this paper presents the use of nonlinear beams to extend the bandwidth of vibration energy harvesters. Fig. 1 shows the 3D geometry of the electrostatic energy harvester analyzed. It includes two fixed electrodes attached to the frame and two variable electrodes on the proof mass suspended by four nonlinear springs which are the key feature of our design. The beams have clamped support on the frame and the other ends are fixed on the proof mass. The geometry of the beams is similar to L-shaped beams, but with a joint angle of 131.2^0. The thickness of the beams or the whole device is $300\,\mu m$. The width and length of the first and second beam are $15\,\mu m$ x $1200\,\mu m$ and $25\,\mu m$ x $200\,\mu m$, respectively, as shown in the right corner of Fig. 1. To obtain the softening regime, four beams are arranged asymmetrically as shown in the Fig. 1. As a result, the spring force versus the displacement of the proof mass was calculated by the finite element method (FEM) in Coventorware as shown in Fig. 2. A softening regime was achieved on one side from about 10 to 90 μm with a quite flat region (very small stiffness) from $30\,\mu m$ to $90\,\mu m$. On the other side it is stiffening.

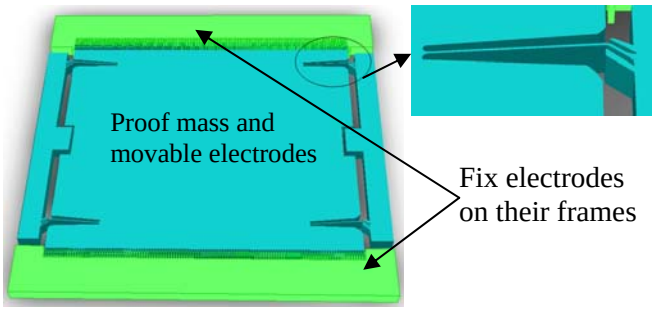

Fig. 1: The 3D layout of electrostatic energy harvester includes two fix electrodes and proof mass suspended by 4 nonlinear springs.

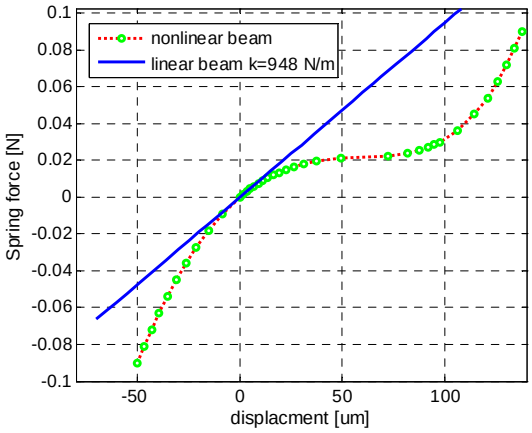

Fig. 2: The spring force vs. displacement of nonlinear springs, calculated by FEM in Coventorware.

ENERGY HARVESTER MODEL

Fig. 3 shows a schematic representation of the energy harvester which is a standard in-plane overlap varying device, except for the springs which are designed to achieve the nonlinear behavior. The model is a generalization of the model in [3]. The

mechanical part consists of the inertial mass m, mechanical damping b represented by a dashpot and the nonlinear beam suspensions. The electrical part consists of two out of phase variable capacitances C_1 and C_2, load resistors R_{L1} and R_{L2}, parasitic capacitances C_{p1} and C_{p2}, load capacitance C_L and an external bias V_e.

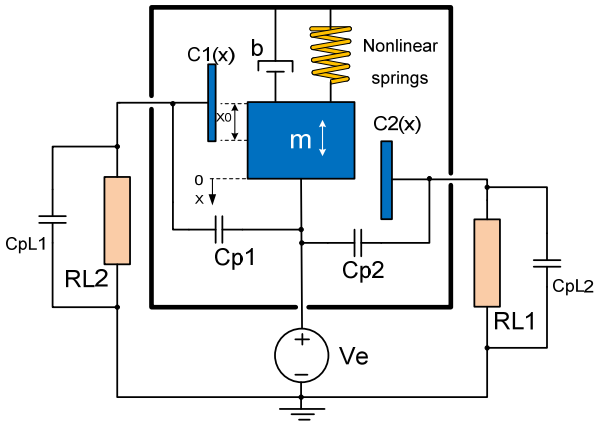

Fig. 3: Electrostatic energy harvester model including the mechanical and electrical part

In modeling of the variable capacitances, we use the parallel plate capacitor formula fit to FEM calculations. The inter-electrode capacitances C_1 and C_2 as functions of the displacement x of the proof mass are

$$C_1(x) = C_{p1} + C_{01}(1-\frac{x}{x_{01}}) \quad (1)$$

$$C_2(x) = C_{p2} + C_{02}(1-\frac{x}{x_{02}}) \quad (2)$$

where C_{01} and C_{02} are the initial capacitances. C_{p1} and C_{p2} represent parasitic capacitances.

The voltages V_{L1} and V_{L2} at the two ports are given by:

$$V_{L1/L2} = \frac{q_{1/2}}{C_{1/2}(x)} + V_e \quad (3)$$

where q_1 and q_2 are the charges on port 1 and port 2 respectively.

Newton's second law describing the motion of the damped mass-spring system is given by

$$m\ddot{x} + b\dot{x} + F_r + F_e = ma \quad (4)$$

Here, m is the mass and ma is the fictitious force. F_e is the electrical force, given by

$$F_e = \frac{1}{2}q_1^2\frac{d}{dx}(\frac{1}{C_1(x)}) + \frac{1}{2}q_2^2\frac{d}{dx}(\frac{1}{C_2(x)}) \quad (5)$$

and F_r is the spring force which is found from FEM and fitted to the polynomial form

$$F_r = \sum_{n=1}^{7} k_n x^n \quad (6)$$

Based on the above equations, the equivalent circuit for the nonlinear spring electrostatic energy harvester is shown in Fig. 4. In SPICE, each variable capacitor $C_{1/2}(x)$ is implemented as an arbitrary fixed capacitor connected in series with a behavioral voltage source [3]. The equivalent circuit includes two sub-circuits for the mechanical part and electrical part respectively. In the mechanical sub-circuit, we chose to split the spring force into the linear term implemented as a capacitor and the remaining nonlinear terms implemented as the behavioral source F_{rn}. We have also implemented a stopper force F_s which is not important at the acceleration levels considered here.

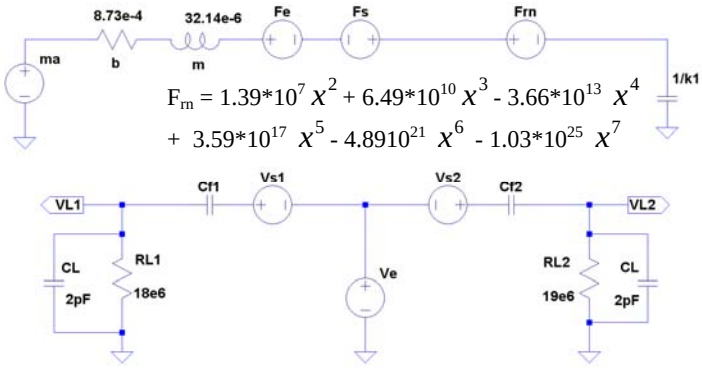

Fig. 4: The equivalent circuit for modeling electrostatic energy harvester.

Table 1: Parameters for nonlinear spring energy harvester.

Parameters	Symbol	Value
Spring constants	k_1	948 N/m
Transducer 1		
Initial finger overlap	x_{01}	110 μm
Initial capacitance	C_{01}	4.67 pF
Parasitic capacitance	C_{p1}	3.74 pF
Transducer 2		
Initial finger overlap	x_{02}	100 μm
Initial capacitance	C_{02}	4.25 pF
Parasitic capacitance	C_{p2}	3.71 pF

RESULTS AND DISCUSSION

In the following we consider a variety of vibration signals: frequency sweeps at fixed amplitude, amplitude sweeps at fixed frequency and broadband random noise with approximately flat power spectral density (PSD).

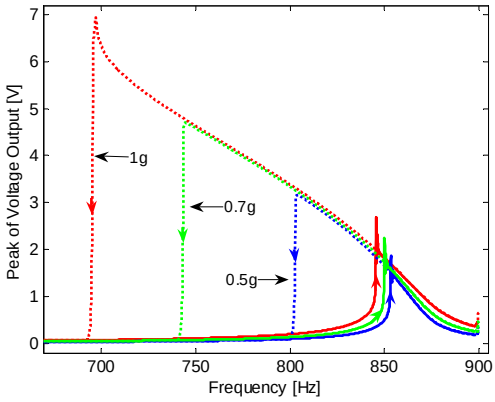

Fig. 5: Up and down frequency sweeps at 0.5g, 0.7g and 1g (peak) excitation with 30V bias. The direction of the arrows shows the direction of the frequency sweeps.

The frequency sweeps are from 600Hz to 900Hz (up-sweep) and from 900Hz down to 600Hz (down-sweep) in 40s. Fig. 5 shows the peak voltage across the first port as a function of frequency. During the forward sweep, the voltage output of the 0.5g (peak) excitation curve jumps up to a higher amplitude at frequency of about 853Hz and decreases with increasing frequency. When performing the frequency sweep downward, the voltage output increases incrementally as the excitation frequency decrease and jumps down to small amplitude value at the frequency of 800Hz, far away from the up-jump frequency, establishes a region of hysteresis or two-valued response. It is evident that two amplitude outputs coexist for any excitation frequency in the range from 800Hz to 853Hz. On increasing the amplitude, the two-valued response region considerably broadens from 743Hz to 850Hz for 0.7g (peak) and from 695Hz to 845Hz for 1g (peak) amplitude excitation. The jump phenomenon in frequency sweeps with the two-valued region appearing on the lower side of the response is a typical property of softening springs.

We also considered frequency sweeps at 0.8g (peak) amplitude excitation for three different bias voltages as shown in Fig. 6. At this level excitation, the voltage output is roughly proportional to the bias voltage away from the jumps. The up-jump frequencies are insensitive to the bias voltage while the down-jump frequencies are roughly insensitive.

Next we consider how the voltage output depends on the vibration amplitude while the driving frequency is kept constant. The driving frequency (840Hz) is selected in the multi-valued response region of the frequency sweeps in Fig 5. The sweeps of amplitude are either from a low to high value (up sweep) or from a high to low value (down sweep) for

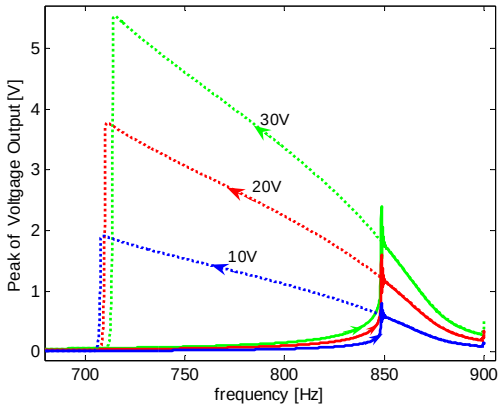

Fig. 6: Up and down frequency sweeps at 0.8g (peak) excitation for 10V, 20V and 30V bias.

three different bias voltages as shown in Fig. 7.

On the up sweep, the voltage output jumps up to the high amplitude value when the excitation reaches 1.4g (peak). After a short transient response, the voltage output continues to increase slowly. On the down sweep, the voltage output stays high beyond 1.4g (peak) where there is also a possible lower amplitude value and drops to small value at about 0.3g (peak). We also see that the jump frequencies are quite independent of the bias voltage. When the device is driven at 840Hz, a two-valued response exists between 0.3g and 1.4g (peak).

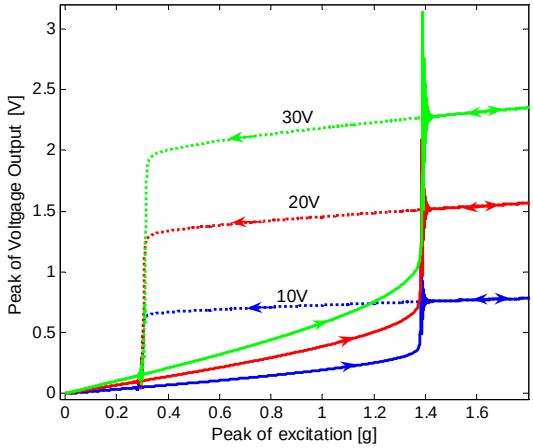

Fig. 7: Up and down amplitude sweeps at 840Hz vibration for 10V, 20V and 30V bias.

Now, we examine the output voltage when the device is driven by broadband random noise. The broadband excitations with a relatively flat PSD from 200Hz to 3000Hz were used. Fig. 8 shows the two-sided output PSD of the first port for many excitation levels from small to large average acceleration PSD values S_a. We notice that the bandwidth of the output considerably widens on increasing excitation (see table 2). Moreover, a shift to the left of the lower

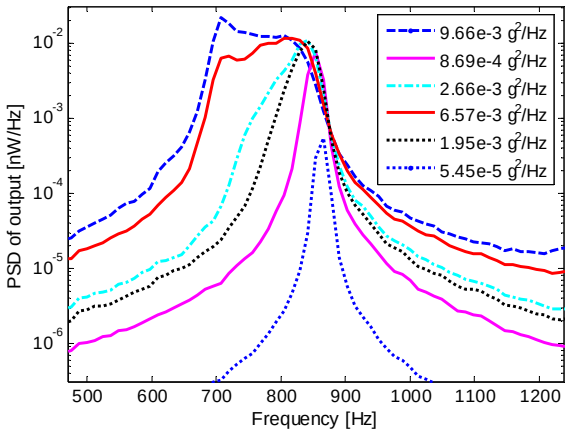

Fig. 8: Two side PSD of output at 30V bias with several levels of the average acceleration PSD

frequency at a half maximum power, f_1, demonstrates that the widening of bandwidth comes from the softening spring effect.

Table 2: The bandwidth of the output PSD for several levels of the acceleration PSD S_a.

S_a (g^2/Hz)	Frequency at a half maximum power f_1 and f_2	Bandwidth $BW = f_2 - f_1$
5.45×10^{-5}	853Hz – 874Hz	21Hz
8.69×10^{-4}	842Hz – 865Hz	23Hz
1.95×10^{-3}	820Hz – 860Hz	40Hz
2.66×10^{-3}	814Hz – 857Hz	43Hz
6.57×10^{-3}	706Hz – 849Hz	143Hz
9.66×10^{-3}	695Hz – 820Hz	125Hz

These results show that the electrostatic energy harvesters utilizing nonlinear springs harvest energy in a much wider bandwidth than the similar energy harvester with linear springs, but it does not necessarily mean that nonlinear spring devices can harvest more (or less) power under wide band vibrations than the linear spring devices can. The average output power of the nonlinear spring harvester is compared with the average output power of a linear spring harvester, both having the same parameters except for the springs ($k_{linear} = k_1 = 948$ N/m, Fig. 2) as shown in Fig. 9. It can be seen that both harvest the same power for the same average acceleration PSD. We know from theory [4] that the effect of mechanical nonlinearities on output power depends on the load resistance. Experiments show that it may enhance performance for certain loads [5], though this is not the case here.

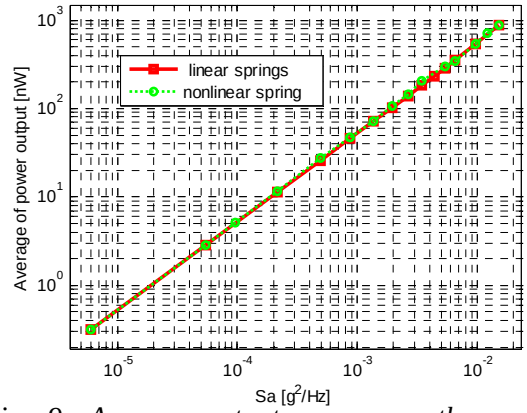

Fig. 9: Average output power vs. the average acceleration PSD for nonlinear and linear springs

CONCLUSION

We have modeled and simulated an energy harvester utilizing nonlinear springs to increase the device bandwidth. For narrowband excitations, we found jumps and multi-valued responses when sweeping either frequency or amplitude. The down sweep bandwidth is greatly enhanced. For broadband excitations, we found a significant bandwidth enhancement with increasing vibration strength while the average output power is the same as for the linear spring device. A prototype is being fabricated at the time of writing and its experimental characterization will be presented in future work.

ACKNOWLEDGEMENT

This work was supported in part by The Research Council of Norway under grant no. 191282.

REFERENCES

[1] Tvedt L G W, Nguyen D S and Halvorsen E 2009 Nonlinear Behavior of an Electrostatic Harvester Under Wide and Narrow Band Excitation (unpublished)

[2] Soliman M S M, Abdel-Rahman E M, El-Saadany E F and Mansour R R 2008 A wideband vibration-based energy harvester *J. Micromech. Microeng.* **18**

[3] Tvedt L G W, Blystad L-C J and Halvorsen E 2008 Simulation of an Electrostatic Energy Harvester at Large Amplitude Narrow and Wide Band Vibrations *Symposium on Design, Test, Integration and Packaging of MEMS/MOEMS - DTIP 2008*

[4] Halvorsen E 2008 Energy Harvesters Driven by Broadband Random Vibrations *J. Microelectromech. Syst.* **17** pp. 1061-1071

[5] Cottone F, Vocca H and Gammaitoni L 2009 Nonlinear Energy Harvesting *Phys. Rev. Lett.* **102** p. 080601